

Augmenting Cats and Dogs: Procedural Texturing for Generalized Pet Tracking

Dominik Borer, Nihat Isik, Jakob Buhmann and Martin Guay

Computer Graphics Laboratory, ETH Zürich, Switzerland

Keywords: Mixed and Augmented Reality, Motion Capture.

Abstract: Cats and dogs being humanity's favoured domestic pets occupy a large portion of the internet and of our digital lives. However, augmented reality technology — while becoming pervasive for humans — has so far mostly left out our beloved pets out of the picture due to limited enabling technology. While there are well-established learning frameworks for human pose estimation, they mostly rely on large datasets of hand-labelled images, such as Microsoft's COCO (Lin et al., 2014) or facebook's *dense pose* (Güler et al., 2018). Labelling large datasets is time-consuming and expensive, and manually labelling 3D information is difficult to do consistently. Our solution to these problem is to synthesize highly varied datasets of animals, together with their corresponding 3D information such as pose. To generalize to various animals and breeds, as well as to the real-world domain, we leverage domain randomization over traditional dimensions (background, color variations and image transforms), but as well as with novel procedural appearance variations in breed, age and species. We evaluate the validity of our approach on various benchmarks, and produced several 3D graphical augmentations of real world cats and dogs using our fully synthetic approach.

1 INTRODUCTION

Augmented reality has the potential to enhance our visual experience of the world with both useful and entertaining information. In the case of animals, we could imagine sharing localized information about our pets, or create amusing augmentations of our favored animals performing stunts, agility parkours and everyday activities such as interrupting a football game. Moreover, animal characters in movies could be tracked and augmented during previs, or motion captured for CG re-enactment.

In order to be able to augment animals with 3D graphical objects from a single RGB camera, we need to be able to automatically estimate the 3D information of the animal in the image. Due to extensive variability in breed, as well as fur appearance and shape, animals are notoriously challenging to track.

While deep learning has allowed un-precedent performance in monocular pose estimation, it has been in large part thanks to large datasets of *hand-labelled* images of *humans*, such as the COCO (Lin et al., 2014) and the MPII (Andriluka et al., 2014) datasets. The problem with these methods is that first it requires vast amounts of hand labelling efforts, and second it is quite challenging to hand-label 3D information

consistently. In consequence, it cannot be used for 3D pose prediction.

In this paper we solve these problems by leveraging the computer graphics toolbox and *synthesizing* a large dataset of animals, labelled with *full 3D* skeleton and camera information. We then design and train a custom deep neural network (DNN) to regress from image to 3D pose. At run-time, we provide our network with a real-world image, and retrieve the 3D information, which we use to add 3D graphical objects on animals such as hats, wings and riders.

The biggest technical challenge with leveraging synthetic data is to bridge the so-called reality gap: the pixel-level difference between real world images and their synthetic counter-parts. DNNs tend to over-fit onto particular features only seen in the synthetic domain, and thereby struggle to generalize to real world data. To address this problem, we employ the strategy of *domain randomization* (Tobin et al., 2017). Thus in the data generation process, we strongly vary dimensions like pose, shape, texture, background, lighting, and camera viewpoint. Another technical challenge to reach the desired 3D augmentations lies in predicting 3D joint orientation and positions that have a good overlay in the augmented image space. While 2D tracking has shown impressive results so far, the exact pixel positions are often lost when going to a 3D pose. We address

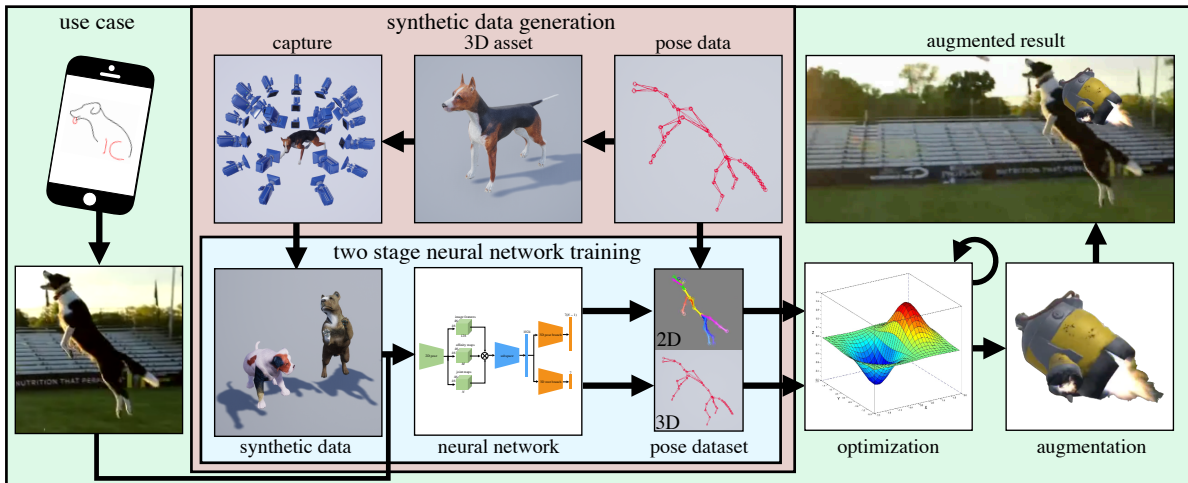


Figure 1: Overview of the proposed approach, which can be divided into 3 basic groups: (red) The data generation process which allows to create a large dataset of synthetic images with according pose information, 2D and 3D. (blue) The step of training a neural network to go from synthetic images to the according pose. (green) Using the trained system to predict an animal’s pose on real world footage, and using those poses to augment the footage with 3D digital assets.

this problem by designing a two step network, producing both 2D and 3D information, which can then be used in an optimization step to create faithful 3D poses from the camera’s viewpoint. As a result, our network is able to generalize to real world data and shows robustness to new environments, shapes, and appearances. The optimized 3D poses are grounded in the camera space allowing us to create entertaining augmentations for cats and dogs in real-world scenarios, as shown in Figure 7.

In Section 4, we discuss the data generation pipeline, Section 5 addresses the network architecture, and in Section 6 the augmentation of the animals is explained.

2 RELATED WORK

The vision of digitally augmenting the real world was first introduced over fifty years ago (Sutherland, 1968), and has since been revisited countless times as progress in hardware, computer vision, and computer graphics continues to be made — each time unlocking new possibilities for communication, education and entertainment.

Several augmentation concepts have already been explored for *humans* around the body, face and hair — allowing people to try virtual make-up and glasses (Javornik et al., 2017), hairs styles (Kemelmacher-Shlizerman, 2016), and clothing (Rogge et al., 2014, Facecake, 2015, Yang et al., 2016). To our knowledge, the only pets augmentation is from *SnapChat*, which we believe

utilize a combination of 2D feature predictions together with the phone’s gyroscope to create 3D augmentation effects, but limited to front-facing dog faces.

To augment animals with 3D objects, we need to estimate their 3D pose. Many techniques for animals build upon methodology developed for human tracking, more specifically 2D landmark or body part estimation (Wei et al., 2016, Newell et al., 2016, Cao et al., 2017, Xiao et al., 2018) from RGB images. A large dataset of images — typically hand-labelled with 2D body part locations — is used to train a multi-stage deep convolutional neural network (DCNN) to predict the confidence location map of each joint or landmark; each stage improving the predictions.

For 3D pose estimation, it is common to train a separate network to go from 2D-to-3D joint locations (Chen and Ramanan, 2017, Tomè et al., 2017, Martinez et al., 2017, Pavlo et al., 2019). We build upon this work and extend it to our use case of animal tracking as described in Section 5.2. Another line of work extends the convolutional network to predict volumetric 3D joint confidence maps (Pavlakos et al., 2016, Mehta et al., 2017), and then optimizes for a kinematic skeleton to match the 3D predictions (Mehta et al., 2017). However, this approach lacks limb orientation, and the sparse set of landmarks can easily lose track of the 3D orientation of the limbs; which could be attenuated by optimizing for a mesh instead of a kinematic skeleton (Xu et al., 2018).

Seeing the progress in human pose estimation, biologists have integrated deep learning based ap-

proaches to track and measure the movements of animals and insects (Kays et al., 2015). Most work in this area is focused on labelling tools for 2D predictions (Graving et al., 2019, Pereira et al., 2018). Some work has focused on modeling the shape of animals (Zuffi et al., 2016) from scans of toy figurines, optimizing for 3D shapes to match 2D joint estimations (Biggs et al., 2018) and capturing their texture from video footage (Zuffi et al., 2018). Recent work combine those approaches in a deep learning framework to estimate Zebra pose, shape and texture (Zuffi et al., 2019) or try to leverage the progress in human pose estimation by transferring it to animals using domain adaptation (Cao et al., 2019).

To avoid manually labelling images, as well as to overcome the challenge of labelling 3D information, many works, both for humans (Chen et al., 2016, Varol et al., 2017, Xu et al., 2019) and animals (Biggs et al., 2018, Mu et al., 2019, Zuffi et al., 2019) have explored generating synthetic datasets.

(Mu et al., 2019) use 3D models to label the images with 2D landmarks, and devised a learning scheme to bridge the reality gap. (Chen et al., 2016) estimate a 3D skeleton from 2D image features, and they include a domain similarity loss to help steer the feature extractor extrapolate to real world imagery. To avoid dealing with the reality gap, (Biggs et al., 2018) create a dataset of silhouettes and regress from silhouettes to 2D keypoints. This unfortunately only performs as good as the given silhouette estimator.

Another way to address the reality gap is by so-called *domain randomization* (Tobin et al., 2017) — to add noise and variations to the dataset to avoid over-fitting. Domain randomization has been shown to achieve state-of-the-art accuracy for car detection (Tremblay et al., 2018, Khirodkar et al., 2018, Prakash et al., 2019), and has unlocked the possibility to use in the real world. In this work, we extend this principle to articulated figures such as animals.

3 OVERVIEW

The core of our approach is a 3D pose predictor from an RGB image. Our overall approach is summarized in Figure 1. While deep neural networks provide state-of-the-art performance for monocular pose estimation, several problems must be overcome in order to be able to track and augment animals.

First, there are no publicly available datasets of animals labeled with 3D skeletons. To solve the data problem, we create a highly varied synthetic dataset of animal images, labeled with 3D information — the

red area in Figure 1. The details of this process are discussed in Section 4.

Second, directly regressing from the 2D image domain to accurate 3D skeletons remains to this day a challenging task. Two strategies help improve our accuracy (blue area in Figure 1). First to perform as much processing as possible in the image domain. Hence we predict 2D joint locations and bone directions as 2D activation maps (Section 5.1), before regressing to 3D. The second strategy is to avoid unnecessary correlations between the 6D rigid (root) prediction and the rest of the body joints, as described in Section 5.2.

The third problem comes from limited GPU memory, which does not allow processing large image frames in real-time. We solve this by estimating a 2D crop when sequentially processing videos. However, the local crop causes our 3D predictions to be in many different *virtual* cameras, as opposed to the footage-capturing camera. To solve this problem, we optimize for a 3D skeleton in the footage-capturing camera space, that seeks to match the 2D predictions, while remaining as similar as possible to the 3D predictions, which is detailed in Section 6. Finally at run-time we attach 3D objects onto the optimized 3D skeleton, as shown in the green area of Figure 1.

4 DATA GENERATION

Our approach leverages modern computer graphics to create a realistic dataset of images I labelled with 3D skeleton information X, Q in camera space, with X representing skeleton coordinates and Q the pose (represented as quaternions). The main challenge for creating realistic images of cats and dogs, lies in their vast variability when it comes to appearance, shape, pose, lighting conditions, and environment. Thus, for any learning framework, over-fitting on a specific animal — not to mention on a synthetic one — is a serious challenge. Additionally, due to the approximate nature of the 3D assets and the rendering algorithms, the learning framework is challenged by a so-called *domain gap*, i.e. the difference between the synthetic training data to the real world test data.

To address the domain gap and over-fitting problems, we leverage the principle of *domain randomization* (Tobin et al., 2017, Tremblay et al., 2018, Khirodkar et al., 2018). Hence, we programmatically introduce a large amount of variability in the most significant dimensions of the dataset, i.e. texture, shape, pose, lighting, and context (or scene background).

This domain randomization can be seen as a regularization or alternatively, as a vast expansion of

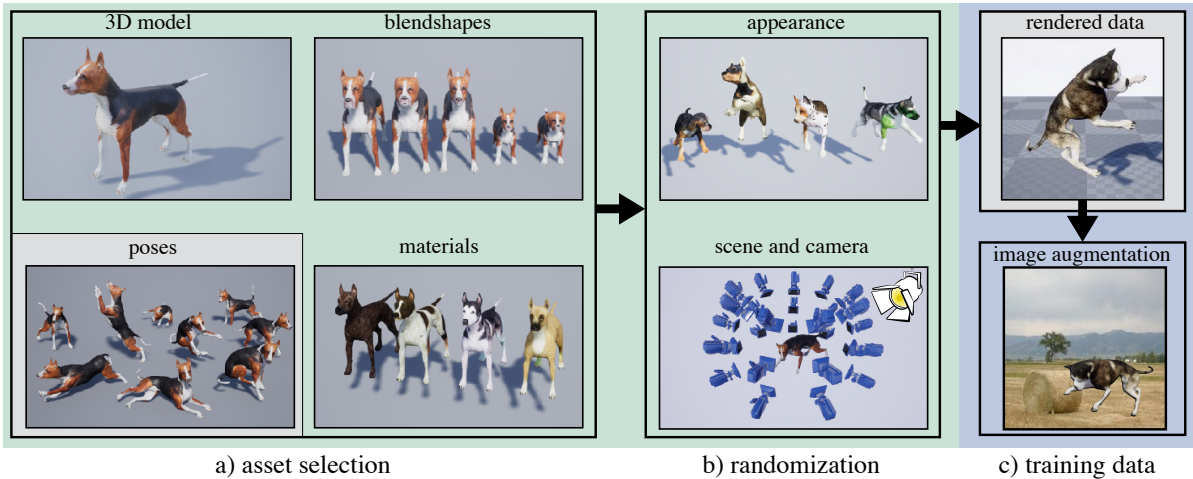


Figure 2: Overview of the data generation pipeline: The pipeline can be split in a 3D part (green) and a 2D part (blue): a) a 3D asset (including mesh, blendshapes, poses, materials), and b) a randomization process where those components are sampled to create a large variation of appearances. Additionally, the scene and camera settings are sampled, leading to the rendered images that are stored together with the pose data (grey). c) During training, standard image augmentations are applied in image space.

the training data distribution that reduces the distance to the real world distribution. Randomizing shape, pose, appearance and lighting requires 3D information and is therefore applied during the animal rendering procedure (Section 4.1). Besides this 3D randomization we apply standard 2D image augmentation techniques such as color space transforms and 2D geometric transforms during training directly in image space (Section 4.2). Without the 2D/3D randomization the model would overfit to the few synthetic animals and not generalize to images of real animals. The overall data generation process is summarized in Figure 2.

4.1 3D Randomization

We utilize a 3D game engine for fast rendering and fast iterations over our datasets. For this purpose, we parameterize the shape and pose of animals with parameters β and Q respectively for shape and pose. Such a parameterization is compatible with real-time game engine rigs, which typically offer only blend shapes and linear blend skinning (LBS) as shape parameterizations.

4.1.1 Shape Parameterization

Our approach starts with a 3D mesh of an animal in a rest pose V_0 , whose shape variations ΔV_j (j different entire meshes) have been hand-crafted for different breeds, age, muscle, fat, bone, etc. We purchased these models on the DAZ platform (DAZ, 2019).

Unlike a small local shape variation such as a muscle bulge, our shape variations for breed and age affect the entire proportions of the mesh, including its underlying skeleton. Hence to remain compatible with LBS, we parameterize the skeleton coordinates X w.r.t. surrounding mesh vertices, which are being deformed by blend shape parameters β_j as follows: $V = V_0 + \sum_j \beta_j \Delta V_j$. For each joint i we choose to linearly map the L closest vertices V^i to the joint position x^i . Hence, we take those mesh vertices in the rest pose V_0^i with the corresponding joint position x_0^i and solve a linear least squares problem: $\|A^i V_0^i + b^i - x_0^i\|$ w.r.t. A^i and b^i . Given a deformed mesh V , the joint positions can then be determined as: $x^i = A^i V^i + b^i$, using the precomputed A^i and b^i .

Following our principles of domain randomization, we sample shape parameters β in a broad range, which not only cover the original artist-intended species, but also various blends between them.

4.1.2 Pose Sampling

In order to robustly track animals in their everyday life, the training data needs to reflect the poses animals tend to perform. Since motion capturing animals is cumbersome, expensive and often times dangerous, we pursue a strategy to leveraging only a sparse set of poses, such as a hand-crafted dataset of about 200 distinct poses; purchased on the DAZ platform (DAZ, 2019).

To sample pose variations, we model a pose distribution using principal component analysis (PCA). The resulting pose vector is then sampled as $Q = P \cdot t$

where P reflects the first K dimensions of the PCA decomposition and t is sampled from a K dimensional multivariate Gaussian.

4.1.3 Appearance Sampling

Naively applying random textures to the appearance of animals will cause the network to disregard important visual cues that appear in texture and help predict the pose, such as the line between the face color and the fur. Hence one can obtain much better results by creating new textures from existing ones — assuming multiple textures in correspondence — by blending between the textures in a seemingly natural way, e.g. part Dalmation and part German Shepherd.

Since uniformly interpolating between two textures leads to washed out colors of both textures, we model texture blending via local patches. We synthesize a 2D blend map $\mathbb{R}^2 \rightarrow \mathbb{R}^1$ using a perceptually natural noise distribution such as Perlin noise (Perlin, 2002). This blending approximates spatially smooth patchwork of species variations in our appearance textures, cf. Figure 2b).

Although our textures do not always exist in the real world, we found that this kind of randomization helps generalizing to new animal appearances not present in the training dataset. Note that we add variations in color space to the rendered images during the training, as detailed later in Section 4.2.

4.1.4 Viewpoint Sampling and Rendering

Lastly, the camera and scene elements such as lights and occluders are sampled.

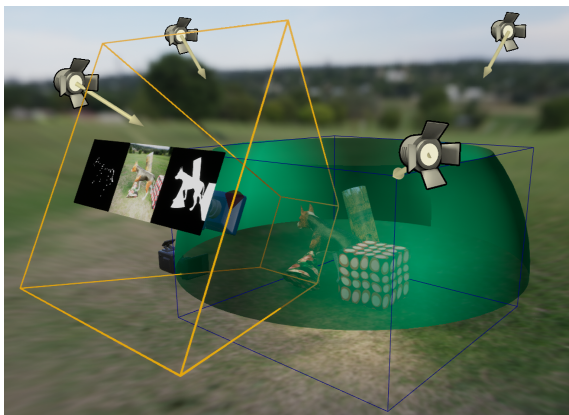


Figure 3: Overview of the render setup: The camera is sampled on the green surface, and then varied within the yellow volume, random meshes are spawned as occluders within the blue capture volume and different light sources are randomized.

Camera. The camera location is sampled on a sphere around the animal with a fixed radius and constraints on azimuth and elevation, illustrated with a green shape in Figure 3. This position then defines the camera orientation, which is aligned with the root of the 3D skeleton. Additionally, a positional offset is sampled in a predefined volume around the camera location, aligned with the camera orientation, (yellow volume in Figure 3) to get the final camera position. Lastly, the camera orientation is varied in a small range to get more out-of-center views.

Lighting. We vary light sources, by sampling colors, intensity, as well as light type between point- and spotlight. Additionally, multiple skylights are blended to achieve a more natural illumination.

Occluders. To be robust to missing body parts, we add occluders defined as random meshes floating in the scene. Their position in the capture space, as well as their orientation, scale, color, and texture is sampled from a predefined range.

4.1.5 Labels

Finally, the image features (RGB-image and mask) are rendered at the desired resolution and saved to disk. The pose parameters Q and the skeleton positions X are mapped into a space relative to the camera. These composed values are then saved together with the camera coordinates, the projection parameters, as well as the 2D coordinates of the skeleton joints.

4.2 2D Randomization

To avoid over-fitting on a specific background, we randomize the context in which animals may appear. We sample random backgrounds, composed with the rendered animal using its 2D mask. The backgrounds are images of natural environments, as well as urban and office settings.

Once overlaid onto a background, the image is further randomized with color space transformations, to account for different brightness, hue, saturation, blur, pixel noise, as well as with geometric transformations such as translation, rotation, scaling and mirroring. Note that we transform the labels according to the geometric transform to maintain the correspondence.¹

¹Note that the set of geometric transforms changes depending on which part of the system is trained (2D vs. 3D), because not all 2D transforms in the image plane can be faithfully mapped to a corresponding transform on the 3D labels.

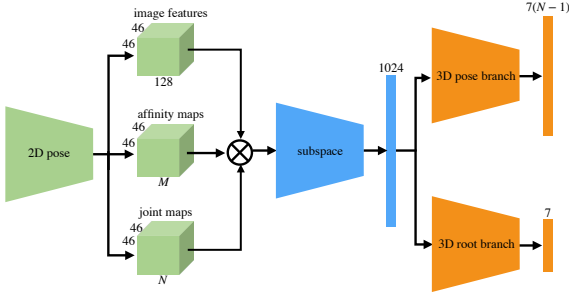


Figure 4: Neural network architecture overview, which consists of three building blocks. First a 2D system (green) that takes images as input and predicts 2D feature maps. Those features are concatenated and with multiple convolutional layers reduced to a lower dimensional subspace (blue). Lastly, two branches (orange) map the subspace to the 3D pose information, with one branch for the root and another for all other joints in a body-centric fashion. Training is done in a two-stage manner: first the 2D part is trained until convergence, before the full system is trained.

5 NETWORK ARCHITECTURE

The result of the data generation process is a dataset of RGB images I of animals at resolution 368×368 , together with their corresponding 2D pixel coordinates $P_X = \{p_1, \dots, p_N\}$, and 3D labels $\{X, Q\} = \{x_1, q_1, \dots, x_N, q_N\}$, with N being the number of joints. This data allows us to design a deep neural network and train it to predict 3D skeleton poses from an input image.

While DNNs have progressed rapidly in recent years, it remains a challenge to regress directly from the image domain to 3D skeletons. Hence we break the problem down into 2D pose feature predictions of 2D joint confidences I^C and 2D joint affinities I^A at resolutions 46×46 , followed by a module that concatenates the 2D features and predicts a 3D skeleton pose X, Q . An overview of this architecture is shown in Figure 4. Examples of joint confidence and affinity maps can be seen in Figure 5 and Figure 6.

5.1 2D Pose Estimation

The 2D part of our network follows the architecture of (Cao et al., 2018), which consists first of a pre-trained feature extractor backbone (in our case VGG (Simonyan and Zisserman, 2015) pre-trained on ImageNet (Deng et al., 2009)), followed by a multi stage convolutional neural network, that refines the predictions over successive stages, with intermediate supervision at each stage (Wei et al., 2016, Cao et al., 2017, Cao et al., 2018). Each stage outputs joint confidence and affinity maps I_{pred}^C, I_{pred}^A and

using the ground truth maps I_{gt}^C, I_{gt}^A we minimize for training the L2 loss:

$$\mathcal{L}(I^C, I^A) = \|I_{pred}^C - I_{gt}^C\|_2^2 + \|I_{pred}^A - I_{gt}^A\|_2^2. \quad (1)$$

5.2 3D Pose Estimation

After the 2D stage, we concatenate the predicted joint confidence maps $I_{46 \times 46 \times N}^C$ with the affinity maps $I_{46 \times 46 \times M}^A$, where M is the number of predicted bones, and the image features $I_{46 \times 46 \times 128}^F$ extracted with the pre-trained feature extractor, and feed them to our 3D-predicting module, which outputs a fixed size 3D skeleton pose vector X, Q .

To avoid learning unnecessary correlations between root and the rest of the pose, we separate the network into two dedicated branches: one for the root, and one for the joints.

In a first step, the concatenated image features and the predicted 2D feature maps are mapped to a lower dimensional latent space ($1 \times 1 \times 1024$) using convolutional blocks each reducing the spatial dimensionality of the features (4x4 convolutions, with stride 2 and padding 2, followed by batch norm and leaky ReLU with slope 0.2). We then feed the fixed size latent vector to the two separate branches (for root and pose), which each have the same fully connected (FC) architecture.

The FC branches follow a resnet type of architecture similar to (Martinez et al., 2017), where linear layers followed by ReLU activation functions are combined with their residual from the previous layer to map to the dimensionality of the pose vector, as shown in Figure 4.

To train the 3D module, we minimize two losses: one for 3D positions X , and one for the orientations Q . Since the orientations are represented as quaternions, we choose an angular distance $d(Q_{pred}, Q_{gt}) = \arccos |\langle Q_{pred}, Q_{gt} \rangle|$, as it is differentiable.

$$\mathcal{L}(X, Q) = \|X_{pred} - X_{gt}\|_2^2 + \lambda \cdot d(Q_{pred}, Q_{gt}), \quad (2)$$

where the weighting λ makes sure that both terms are equally weighted.

5.3 Training Details

Data Details. In order to reduce redundancies of pose and viewpoints, the pose data is not represented in global world coordinates, but transformed into camera coordinates. Additionally, the pose is represented in a *body frame* representation, which factors out the root position and orientation for all other joints. Hence, the same pose in different positions and

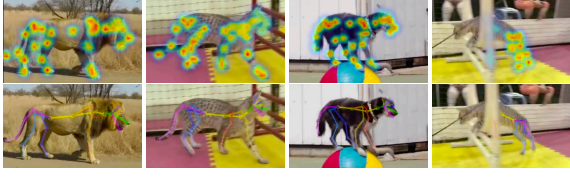


Figure 5: Example outputs of the 2D network (joint maps on top) and the inferred 2D skeleton (bottom). The most right example shows a common problem with occlusions which can easily occur for animals the size of a cat.

root orientations does not vary. Note, the body frame representation also leads to a decoupling of the cost and thereby the gradients in the two branches. To get back to the camera space, the predicted joint positions and orientations are combined with the predicted root pose, as follows:

$$\hat{X}^i = X_{pred}^{root} + X_{pred}^i \quad \text{and} \quad \hat{Q}^i = Q_{pred}^{root} \cdot Q_{pred}^i. \quad (3)$$

Hardware and Learning Settings. We generate a dataset of 100k samples, covering a wide range of randomizations. The 3D positions and orientations are normalized to zero mean and unit standard deviation, the input images are normalized using the pre-computed statistics from ImageNet (Deng et al., 2009) and the joint- and affinity-maps are not normalized. Each model, 2D and 3D, is then trained on the entire dataset for 100 epochs, using the Adam optimizer (Kingma and Ba, 2015) with an initial learning rate of $1e-4$, and a decay factor of 0.5 every 20 epochs, with a mini-batch of size 16. The training of each module takes about three days on an NVIDIA Titan Xp (12GB).

6 TRACKING AND AUGMENTATION

Taking an image as input, our network outputs 2D feature maps (joint confidence maps I^C and affinity maps I^A), together with a 3D skeleton of the pose X, Q . There are two challenges that prevent us from directly using the 3D pose for augmenting graphical elements. The first is that our model was trained specifically for images of size 368×368 (capped by current GPUs memory size) and we cannot track an animal in a full larger frame. The second aspect is how deep neural networks map the 3D space. It behaves in a nearest neighbor fashion leading to 3D predictions which seem natural, but are not “spot on” with regard to the joints in image space.

To solve these challenges, we first utilize a crop to track in a full image space, and then perform an optimization in 3D for a pose that matches best the 2D

features, while remaining close to the 3D pose in our crop. Note that optimizing directly for 2D predictions would cause spurious poses due to a lack of 3D constraints, and would be challenged by global detection (prediction of the overall orientation of the body and limbs).

Assuming a run-time frame is of size $\hat{I}_{1920 \times 1080}$. At the first frame, we utilize the fully convolutional part of our network which predicts the 2D maps, and estimate a crop position and size. The subsequent frames $\hat{I}(t)$ will use the previous frame’s $\hat{I}(t-1)$ predictions to predict the next crop.

Using the crop, we feed the cropped image to our network and retrieve the 3D pose X, Q , as well as the 2D feature maps I^C, I^A . Using the feature maps and the graph-based inference of (Cao et al., 2017), we compute 2D skeleton joint positions $\hat{P}_X = \{p_1, \dots, p_N\}$ in the full image space. Now we solve for a new pose Q' and root position X'_{root} as to be similar to the 3D predictions, while conforming to the 2D predictions as much as possible w.r.t. the projected 3D joint locations in image space $Proj(\Phi(Q', X'_{root}))$:

$$\arg \min_{Q', X'_{root}} \left\| Proj(\Phi(Q', X'_{root})) - \hat{P}_X \right\| + \lambda_Q \cdot d(Q, Q'), \quad (4)$$

where $\Phi(Q)$ computes the positions P_X through forward kinematics (bone lengths are determined from the predicted positions X).

6.1 Graphics Augmentation

With the 3D skeleton, we can attach rigid objects to joints and transform them using the joint position and orientation.

We scale the object based on the average depth of the skeleton, and length of the body defined as the pelvis joint to the neck joint.

Rigid objects in their identity transform may not be aligned with the body’s features. For example, a hat needs to be aligned with the head and oriented as to be sitting on the head. We utilize a template model that we dress with all types of augmentations: a hat, a rider, etc. We pose the object into a transform $\hat{T}(0)$, and then compute the transform between the template rig transform and the object’s transform, resulting in $T^{-1}(0)\hat{T}(0)$.

At runtime, we have a predicted joint transform $T(t)$ and the objects position and orientation is thus: $\hat{T}(t) = T(t)T^{-1}(0)\hat{T}(0)$.

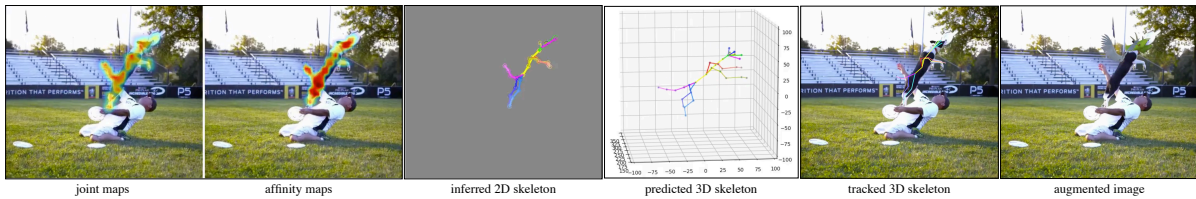


Figure 6: Overview of the different intermediate results along the system.

7 RESULTS AND DISCUSSION

7.1 Data

Using our data generation pipeline, we were able to generate seemingly realistic images of animals covering a wide and diverse range of variations, as shown in Figure 2 and accompanying video. Our new and diverse dataset allowed us to successfully train a neural network that is capable of generalizing to real — never seen before — images of animals. One of the keys to our success is the flexibility and speed of our approach, which allowed us to iterate quickly our data. We experimented with both a dog dataset comprised of German shepherd, wolf, bull terrier, etc., and a dataset of felines comprised of lion, tiger, cheetah, etc. We trained models on each individual dataset, as well as on mix of both (dog and cat). While the models from the individual datasets perform well for the respective species, the mixed dataset outperformed both, which further strengthens the principle of domain randomization.

7.2 Network

The 2D pose estimation part of our network (green part in Figure 4) is capable of predicting qualitatively accurately various dog breeds and feline species, both seen and unseen in our training data. As can be seen in the first three columns of Figure 5 and in Figure 6, the 2D predictions of the joint confidence and affinity maps, as well as the resulting inferred 2D skeleton, have an accurate overlap with the body parts in the image. But large occlusions can still be problematic as can be seen in the last column in Figure 5.

The 3D pose estimation part (blue and orange part in Figure 4) is still challenging, especially when the pose space is hard to model. Due to the lack of large amounts of pose data (for example mocap), we synthetically increased the pose space by vastly sampling a PCA space, created from our 200 pose samples. Hence, while the predicted 3D poses still lack in perfect overlap with the images, they clearly reflect the

overall action of the animal, as we can see in the 3D plot of Figure 6.

Finally, it is worth mentioning that splitting up the training into two parts: first the 2D part of the network, followed by the 3D part, was crucial. Training the entire model end-to-end did not converge to the same level of accuracy.

7.3 Augmentations

One of the main benefits of our network and dataset is that we can predict not only 3D positions, but also 3D orientations of the body parts. Hence we can create graphical augmentations with objects that both move and rotate along the animal, which was never seen before — as shown in our accompanying video and Figure 7.

For example, we thought that if a cat running on a football field was entertaining enough to make the news, it would be even funnier once augmented with a football helmet on its head and a jet-pack on its spine. We can see on social media people posting vast amounts of videos with their dog performing stunts or agility parkour. For example, someone might throw an object and have their dog catch it in mid-air. We augmented such stunts with a jet pack, worn on the back, and with animated angel wings, making it seem like the dog could fly.

To demonstrate the possibility of exhibiting secondary dynamics onto another object, we added a cowboy rider onto a white cat as to look like he is performing rodeo. The rider is modelled as an articulated character with elastic dynamics on the joints with decreasing stiffness as we get further away from the hip joints. As the cat spine moves and rotates, the rider follows in a delayed fashion.

7.4 Evaluation

The lack of large public animal datasets limit the options for quantitative evaluation and comparison to related work. The two animal datasets we are aware of (Biggs et al., 2018, Cao et al., 2019), are both relatively small and only provide 2D annotations. Our



Figure 7: Augmentation results on a variety of dogs and cats performing everyday activities including stunts with their beloved owners.

skeleton has more joints and hence we can only compare on a subset, which includes 3 joints per leg and the tail and the facial keypoints, ignoring head, neck, spine, shoulders and hips. The small discrepancies in the exact positioning of joints cause additional evaluation errors. Despite having trained only on dogs and felines, for completeness we evaluate on all provided animal categories.

The first dataset (Biggs et al., 2018) consists of short video sequences of various animals annotated with keypoints and silhouette. While their approach requires a silhouette extractor, our model predicts from the raw image. As can be seen in Table 1, for the dog sequences we outperform their raw confidence map result and achieve similar accuracy as their optimized result.

Table 1: Comparison to (Biggs et al., 2018) using the *Percentage of Korrekt Keypoints (PCK)* metric, with threshold $d = 0.2 \cdot \sqrt{|S|}$, where $|S|$ is the area of the silhouette. While their confidence map result (Raw) is further optimized using quadratic programming (QP) or genetic algorithm (GA), our result comes from the graph based inference.

	(Biggs et al., 2018)			Ours	
	Raw	QP	GA	All	Visible
dog	66.9	66.6	66.9	70.5	77.5
rs_dog	64.2	63.4	81.2	77.0	79.6
bear	83.1	83.7	88.9	79.4	85.9
camel	73.3	74.1	87.1	56.6	39.2
cow	89.2	88.4	94.7	80.8	90.6
horsejump-high	26.5	27.7	24.4	50.6	53.9
horsejump-low	26.9	27.0	31.9	50.0	51.6
impala	-	-	-	86.4	86.4

The second dataset (Cao et al., 2019) is based on Pascal VOC 2011 (Everingham et al.,), extended with keypoint annotations for various animal cate-

gories. While their approach requires a large-scale human pose dataset, a smaller animal pose dataset and an animal bounding box dataset, our approach only requires synthetic data, which is much cheaper to create than an, albeit small, real animal pose dataset. As can be seen in Table 2, for the dog dataset we achieve similar performance.

Table 2: Comparison to (Cao et al., 2019) using the *Mean Average Precision (mAP)* metric. While for the dog dataset we achieve similar performance, it does not generalize as well to other categories. The cat dataset consists of a lot of very closeup views and furry cats, which differs from our synthetic data, and hence explains the low performance. For other categories the error can be explained due to missing predictions rather than incorrect predictions.

	(Cao et al., 2019)	mAP		
		@0.5	@0.75	Total
dog	41.0	62.9	37.9	38.9
cat	42.3	31.1	13.1	15.0
sheep	54.7	48.3	32.6	33.0
cow	57.3	36.1	17.2	18.4
horse	53.1	60.2	40.2	38.0

Note that the PCK metric only measures the accuracy of the predicted keypoints, while mAP also considers missed predictions, which explains the difference between the two datasets.

Due to the lack of 3D annotations, we evaluate our model on unseen synthetic sequences. As can be seen in Table 3, for synthetic data the 2D estimator is extremely accurate, while the 3D estimator still suffers from significant errors, especially when the animal is turning away/towards the camera, compared to a simpler side view.

Table 3: Evaluation on unseen synthetic sequences. For the 2D evaluation we use the PCKh metric, where the head segment spans from the back of the head to the tip of the nose, and to evaluate the 3D performance we report the *Mean Per Joint Position Error (MPJPE)*.

	2D, PCKh			3D, MPJPE
	@1.0	@0.5	@0.1	
Walking	99.2	98.6	86.4	19.3
Running	99.9	99.5	90.6	19.3
Sprinting	99.5	98.9	87.5	18.1
Turning	99.5	98.1	79.9	47.8

7.5 Discussion

While we were able to automatically augment many videos of animals, there remains much room for improvement. For example, our predictions still suffer from complex occlusions, motion blur, or from a large discrepancy with the breeds we used in our datasets. For instance, presenting an extremely furry dog caused our network to produce spurious predictions.

Predicting 3D poses from 2D image features such that the predicted 3D joints overlap accurately with the 2D body in the image, remains a challenge in computer vision. The 3D predictions are often “smoothed out” and seem to hold a strong bias towards the mean pose. Most trackers will then correct this with an optimizer as a post process — as we did in this work. In the future, it would be better to have a cross domain (pixel to pose) capabilities as to facilitate or even remove the last refinement step.

We currently estimate 2D joint confidence maps in a bottom up fashion, but consider only and trained only for individual 3D poses. Moving forward, it would be interesting to track and augment multiple animals in a scene.

Finally, our synthetic data generates not only 3D poses, but also UV maps, normals, depth, as well as mesh vertices. In the future we would like to explore techniques that can leverage this dense information, as well as texture-related augmented reality.

8 CONCLUSION

By fully pursuing the principles of domain randomization, we procedurally synthesized a large dataset of cats and dogs with many variations in breeds and species, and were able to demonstrate the possibility of automatically tracking and augmenting real world animals, with synthetic data only — no animals were hurt in the making of this experiment. In the future,

we would like to improve the accuracy of our 3D predictions and conceive more compact models deployable on mobile devices.

REFERENCES

- Andriluka, M., Pishchulin, L., Gehler, P., and Schiele, B. (2014). 2d human pose estimation: New benchmark and state of the art analysis. In *IEEE Conference on Computer Vision and Pattern Recognition (CVPR)*.
- Biggs, B., Roddick, T., Fitzgibbon, A., and Cipolla, R. (2018). Creatures great and SMAL: Recovering the shape and motion of animals from video. In *ACCV*.
- Cao, J., Tang, H., Fang, H.-S., Shen, X., Lu, C., and Tai, Y.-W. (2019). Cross-domain adaptation for animal pose estimation. In *The IEEE International Conference on Computer Vision (ICCV)*.
- Cao, Z., Hidalgo, G., Simon, T., Wei, S., and Sheikh, Y. (2018). Openpose: Realtime multi-person 2d pose estimation using part affinity fields. *CoRR*, abs/1812.08008.
- Cao, Z., Simon, T., Wei, S.-E., and Sheikh, Y. (2017). Real-time multi-person 2d pose estimation using part affinity fields. In *CVPR*.
- Chen, C.-H. and Ramanan, D. (2017). 3d human pose estimation = 2d pose estimation + matching. *2017 IEEE Conference on Computer Vision and Pattern Recognition (CVPR)*, pages 5759–5767.
- Chen, W., Wang, H., Li, Y., Su, H., Tu, C., Lischinski, D., Cohen-Or, D., and Chen, B. (2016). Synthesizing training images for boosting human 3d pose estimation. *CoRR*, abs/1604.02703.
- DAZ (2019). Daz big cat 2 and millennium dog. <https://www.daz3d.com/daz-big-cat-2>, <https://www.daz3d.com/mighty-king-poses-for-the-daz-lion>, <https://www.daz3d.com/millennium-dog-bundle>, <https://www.daz3d.com/ultimate-canine-bundle>.
- Deng, J., Dong, W., Socher, R., Li, L.-J., Li, K., and Fei-Fei, L. (2009). ImageNet: A Large-Scale Hierarchical Image Database. In *CVPR09*.
- Everingham, M., Van Gool, L., Williams, C. K. I., Winn, J., and Zisserman, A. The PASCAL Visual Object Classes Challenge 2011 (VOC2011) Results. <http://www.pascal-network.org/challenges/VOC/voc2011/workshop/index.html>.
- Facecake (2015). Swivel.
- Graving, J. M., Chae, D., Naik, H., Li, L., Koger, B., Costelloe, B. R., and Couzin, I. D. (2019). Fast and robust animal pose estimation. *bioRxiv*.
- Güler, R. A., Neverova, N., and Kokkinos, I. (2018). Densepose: Dense human pose estimation in the wild. In *Proceedings of the IEEE Conference on Computer Vision and Pattern Recognition*, pages 7297–7306.
- Javornik, A., Rogers, Y., Gander, D., and Moutinho, A. M. (2017). Magicface: Stepping into character through an augmented reality mirror. In *Proceedings of the 2017 CHI Conference on Human Factors in Computing Systems*, CHI ’17, pages 4838–4849.

- Kays, R., Crofoot, M. C., Jetz, W., and Wikelski, M. (2015). Terrestrial animal tracking as an eye on life and planet. *Science*, 348(6240).
- Kemelmacher-Shlizerman, I. (2016). Transfiguring portraits. *ACM Trans. Graph.*, 35:94:1–94:8.
- Khirodkar, R., Yoo, D., and Kitani, K. M. (2018). Domain randomization for scene-specific car detection and pose estimation. *CoRR*, abs/1811.05939.
- Kingma, D. P. and Ba, J. (2015). Adam: A method for stochastic optimization. In *3rd International Conference on Learning Representations, ICLR 2015, San Diego, CA, USA, May 7-9, 2015*.
- Lin, T.-Y., Maire, M., Belongie, S., Hays, J., Perona, P., Ramanan, D., Dollár, P., and Zitnick, C. L. (2014). Microsoft coco: Common objects in context. In *European conference on computer vision*, pages 740–755. Springer.
- Martinez, J., Hossain, R., Romero, J., and Little, J. J. (2017). A simple yet effective baseline for 3d human pose estimation. *2017 IEEE International Conference on Computer Vision (ICCV)*, pages 2659–2668.
- Mehta, D., Sridhar, S., Sotnychenko, O., Rhodin, H., Shafiei, M., Seidel, H.-P., Xu, W., Casas, D., and Theobalt, C. (2017). Vnect: Real-time 3d human pose estimation with a single rgb camera. *ACM Trans. Graph.*, 36(4):44:1–44:14.
- Mu, J., Qiu, W., Hager, G., and Yuille, A. (2019). Learning from synthetic animals.
- Newell, A., Yang, K., and Deng, J. (2016). Stacked hour-glass networks for human pose estimation. In *ECCV*.
- Pavlakos, G., Zhou, X., Derpanis, K. G., and Daniilidis, K. (2016). Coarse-to-fine volumetric prediction for single-image 3d human pose.
- Pavlo, D., Feichtenhofer, C., Grangier, D., and Auli, M. (2019). 3d human pose estimation in video with temporal convolutions and semi-supervised training. In *Conference on Computer Vision and Pattern Recognition (CVPR)*.
- Pereira, T., Aldarondo, D. E., Willmore, L., Kislin, M., Wang, S. S.-H., Murthy, M., and Shaevitz, J. W. (2018). Fast animal pose estimation using deep neural networks. *bioRxiv*.
- Perlin, K. (2002). Improving noise. *ACM Trans. Graph.*, 21(3):681–682.
- Prakash, A., Bochoon, S., Brophy, M., Acuna, D., Cameracci, E., State, G., Shapira, O., and Birchfield, S. (2019). Structured domain randomization: Bridging the reality gap by context-aware synthetic data. In *International Conference on Robotics and Automation, ICRA 2019, Montreal, QC, Canada, May 20-24, 2019*, pages 7249–7255.
- Rogge, L., Klose, F., Stengel, M., Eisemann, M., and Magnor, M. (2014). Garment replacement in monocular video sequences. *ACM Trans. Graph.*, 34(1):6:1–6:10.
- Simonyan, K. and Zisserman, A. (2015). Very deep convolutional networks for large-scale image recognition. In *International Conference on Learning Representations*.
- Sutherland, I. E. (1968). A head-mounted three dimensional display. In *AFIPS Fall Joint Computing Conference*, pages 757–764.
- Tobin, J., Fong, R., Ray, A., Schneider, J., Zaremba, W., and Abbeel, P. (2017). Domain randomization for transferring deep neural networks from simulation to the real world. *CoRR*, abs/1703.06907.
- Tomè, D., Russell, C., and Agapito, L. (2017). Lifting from the deep: Convolutional 3d pose estimation from a single image. *2017 IEEE Conference on Computer Vision and Pattern Recognition (CVPR)*, pages 5689–5698.
- Tremblay, J., Prakash, A., Acuna, D., Brophy, M., Jampani, V., Anil, C., To, T., Cameracci, E., Bochoon, S., and Birchfield, S. (2018). Training deep networks with synthetic data: Bridging the reality gap by domain randomization. *CoRR*, abs/1804.06516.
- Varol, G., Romero, J., Martin, X., Mahmood, N., Black, M. J., Laptev, I., and Schmid, C. (2017). Learning from synthetic humans. *2017 IEEE Conference on Computer Vision and Pattern Recognition (CVPR)*.
- Wei, S.-E., Ramakrishna, V., Kanade, T., and Sheikh, Y. (2016). Convolutional pose machines. In *CVPR*.
- Xiao, B., Wu, H., and Wei, Y. (2018). Simple baselines for human pose estimation and tracking. In *European Conference on Computer Vision (ECCV)*.
- Xu, W., Chatterjee, A., Zollhöfer, M., Rhodin, H., Mehta, D., Seidel, H.-P., and Theobalt, C. (2018). Monopercap: Human performance capture from monocular video. *ACM Trans. Graph.*, 37(2).
- Xu, Y., Zhu, S.-C., and Tung, T. (2019). Denserac: Joint 3d pose and shape estimation by dense render-and-compare. In *The IEEE International Conference on Computer Vision (ICCV)*.
- Yang, S., Ambert, T., Pan, Z., Wang, K., Yu, L., Berg, T. L., and Lin, M. C. (2016). Detailed garment recovery from a single-view image. *CoRR*, abs/1608.01250.
- Zuffi, S., Kanazawa, A., Berger-Wolf, T., and Black, M. J. (2019). Three-d safari: Learning to estimate zebra pose, shape, and texture from images “in the wild”. In *International Conference on Computer Vision*.
- Zuffi, S., Kanazawa, A., and Black, M. J. (2018). Lions and tigers and bears: Capturing non-rigid, 3D, articulated shape from images. In *IEEE Conference on Computer Vision and Pattern Recognition (CVPR)*. IEEE Computer Society.
- Zuffi, S., Kanazawa, A., Jacobs, D., and Black, M. J. (2016). 3d menagerie: Modeling the 3d shape and pose of animals.